Direct strain and elastic energy evaluation in rolled-up semiconductor tubes by x-ray microdiffraction

A. Malachias,[1,2,*] Ch. Deneke,[3] B. Krause,[4] C. Mocuta,[2] S. Kiravittaya,[1] T. H. Metzger,[2] and O. G. Schmidt[1,3]
[1]*Max-Planck-Institut für Festkörperforschung, Heisenbergstrasse 1, D-70569 Stuttgart, Germany*
[2]*European Synchrotron Radiation Facility, BP 220, F-38043 Grenoble Cedex, France*
[3]*Institute for Integrative Nanosciences, IFW Dresden, Helmholtzstrasse 20, D-01069 Dresden, Germany*
[4]*Institut für Synchrotronstrahlung, Forschungszentrum Karlsruhe, Postfach 3640, 76021 Karlsruhe, Germany*
(Received 5 September 2008; revised manuscript received 17 November 2008; published 5 January 2009)

We depict the use of x-ray diffraction as a tool to directly probe the strain status in rolled-up semiconductor tubes. By employing continuum elasticity theory and a simple model, we are able to simulate quantitatively the strain relaxation in perfect crystalline III-V semiconductor bilayers and multilayers as well as in rolled-up layers with dislocations. The reduction in the local elastic energy is evaluated for each case. Limitations of the technique and theoretical model are discussed in detail.

DOI: 10.1103/PhysRevB.79.035301 PACS number(s): 61.05.cp, 61.46.−w

I. INTRODUCTION

The ability to release and transfer semiconductor layers with high crystalline quality has lead to additional possibilities for the fabrication of devices on the microscale and nanoscale.[1] Strain properties can be exploited to produce bending of the layer, leading to a repositioning of a predefined film area[2,3] or curling into rolled-up tubes.[4,5] In these structures the partial release of the flat layer strain results in a significant change of the lattice configuration, modifying properties such as semiconductor band-gap energies[6,7] and charge-carrier mobilities.[8,9] Rolled-up semiconductor microtubes/nanotubes can be used as flexible ring resonators[10–12] as well as on-chip integrative refractometers,[13] linear fluidic devices,[14,15] and mechanical components.[16,17]

A general layer design that is often used for producing rolled-up structures consists in the heteroepitaxy of two or more pseudomorphically grown thin films on top of an etchant-sensitive layer. Selective etching is then used to release the top layers that relax elastically by rolling up into a tube, as depicted in Fig. 1(a). Since the process depends only on the pre-existence of a strain gradient across the layers,[18] it can be generalized for obtaining a heterostructure that combines different compounds such as organic/semiconductor,[19] oxide/semiconductor,[12] metal/semiconductor,[20,21] or combinations thereof[2] into a self-assembled radial multilayer. Such possibility is, in fact, one of the driving forces for research in this field. However, for applications in material integration and optoelectronic structures, the precise knowledge of local strain in rolled-up layers is crucial for band-gap engineering, as well as for the fine tuning of strain dependent electric and magnetic properties and for layer-to-layer interface optimization.

Structural characterization of single rolled-up tubes has been carried out mainly by microscopy methods such as scanning electron microscopy (SEM) and transmission electron microscopy (TEM). SEM is generally the technique of choice in providing insights on the tube radius, morphology, and layer folding quality[2] while TEM has been successfully used in studying interfaces between successive windings.[19–21] Average strain can be obtained from micro-Raman measurements without a clear distinction of the strain components in each direction.[22–24] Despite the information available from these techniques, a complete scenario describing the strain relaxation inside tubes and correlating its mesoscopic and crystalline properties could only be drawn recently by using x-ray microdiffraction, which allows for directly measuring the radial lattice-parameter distribution over the rolled-up layers.[25]

For this work $In_xAl_yGa_{1-x-y}As/GaAs$ ($x \leq 0.33$, $y \leq 0.2$) epitaxial layers were grown on top of an etchant-sensitive (sacrificial) AlAs layer on GaAs(001) substrates.[26] After rolling, the lattice-parameter configuration inside single tubes is retrieved by x-ray microdiffraction. The paper is organized as follows. First we discuss a model based on continuum elastic theory which is used to obtain the local strain status in a rolled-up tube. The result is compared with models available in the literature. Second we describe the sample design and use of x-ray microbeam as a probe in studying strain relaxation in single tubes. The reciprocal space configuration and alignment procedure are discussed. A simple x-ray model that holds for extracting quantitative information is shown. Finally x-ray measurements performed in rolled-up III-V semiconductor tubes are simulated, allowing the direct evaluation of local strain and elastic energy.

II. ELASTICITY THEORY

The rolling up of pseudomorphically strained thin films is driven by the minimization of the total elastic energy E as described in Refs. 25–29. For epitaxially grown cubic crystals without torsion components, E is locally given by[27,28]

$$E(r) = \frac{C_{11}(r)}{2}(\varepsilon_x^2 + \varepsilon_y^2 + \varepsilon_z^2) + C_{12}(r)(\varepsilon_x\varepsilon_y + \varepsilon_x\varepsilon_z + \varepsilon_z\varepsilon_y), \tag{1}$$

where the subscripts x, y, and z indicate directions that are parallel to the main crystallographic axes. The dependence of the elastic constants on the local composition at the position r is explicitly shown in Eq. (1) for C_{11} and C_{12} and implicit

 ©2009 The American Physical Society

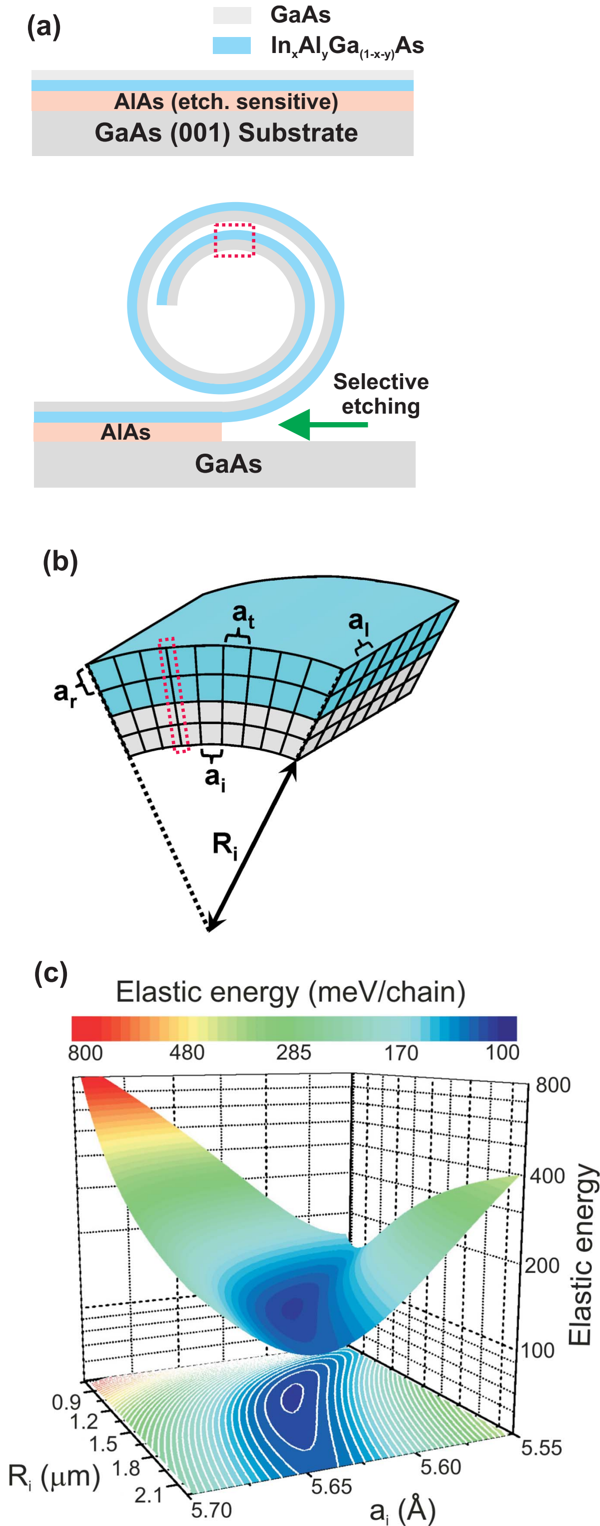

FIG. 1. (Color online) (a) Schematic of the rolling up of a bilayer semiconductor tube. (b) Sketch of the lattice-parameter components and radius of a section from the inner turn of a bilayer tube [zoom of dashed rectangle area of (a)]. See text for discussion. (c) Elastic energy of an atomic chain in the radial direction—sketched as the dashed red rectangle in (b)—evaluated in the R_i–a_i parameter space for a 200 Å $In_{0.2}Ga_{0.8}As$/200 Å GaAs bilayer.

for the strain components. In the following paragraphs the subscripts x, y, and z for the planar layer will be referred to, respectively, as t (tangential), l (longitudinal), and r (radial) for clarity.

If such an epitaxial single crystalline film is curved into a defect-free cylinder with inner radius R_i, the lattice parameter in the tangential (a_t) direction varies continuously inside the layers. The local value of a_t at the position r with respect to the tube inner surface is given by[29]

$$a_t(r) = a_i(1 + r/R_i), \tag{2}$$

where a_i is the tangential lattice parameter of the inner surface as shown in Fig. 1(b). One should note that Eq. (2) is valid only for $r \ll R_i$, which is the case for nanometer-thick layers in rolled cylinders of micrometer-sized diameters. After the releasing of the layers the crystalline lattice is allowed to expand (or contract) in the radial (z) direction and the three strain components are then related by the plane strain condition,

$$\varepsilon_r = -[C_{12}/C_{11}](\varepsilon_t + \varepsilon_l). \tag{3}$$

It is possible, hence, to obtain the final configuration for a given rolled-up tube by minimizing the total elastic energy for its layer structure. By replacing Eqs. (2) and (3) into Eq. (1), one can rewrite the total elastic energy for a stack of N layers as

$$E_{\text{tot}}(a_i,R_i,\varepsilon_l) = \sum_{n=0}^{N-1} \int_{d_n}^{d_{n+1}} E(a_i,R_i,\varepsilon_l,r)dr, \tag{4}$$

where the index $n=0$ denotes the bottom interface of the first layer in the stack ($d_0=0$) and d_n are the positions of the interfaces in the layer stack using d_0 as a reference. For a fixed longitudinal strain ε_l the values of R and a_i that minimize E_{tot} for an atomic chain aligned perpendicularly to the tube surface, as sketched by the dashed red rectangle in Fig. 1(b), can be found numerically by evaluating Eq. (4) in a range of the configuration space of a_i and R_i. Figure 1(c) shows a three-dimensional (3D) plot of E_{tot} for a selected bilayer configuration consisting of 200 Å $In_{0.2}Ga_{0.8}As$/200 Å GaAs (therefore $N=2$, $d_1=200$ Å, and $d_2=400$ Å) with $a_l=a_{\text{GaAs}}=5.653$ Å in a limited configuration-space window. The position of the minimum indicates the equilibrium state for the tube, which is obtained by the conditions

$$\partial E_{\text{tot}}/\partial a_i = 0, \quad \partial E_{\text{tot}}/\partial R_i = 0. \tag{5}$$

Analytical solutions for $N=2$ and multilayer cases are given in Refs. 29 and 27, respectively. The values of a_i and R_i obtained here from direct energy minimization using Eq. (4) via numerical methods are in quantitative agreement with those obtained from the analytical solutions from Refs. 22, 27, and 29 within an error bar of ±1%. A numerical minimization of Eq. (4) allows additionally for an evaluation of the equilibrium conditions with any combination of fixed parameters (e.g., fixing R_i to the experimentally observed radius) instead of restricting the process to a_i and R_i from the predicted equilibrium.

III. EXPERIMENTAL

A. Samples and layer layout

Selected samples were chosen to evidence how different layer configurations affect the lattice relaxation inside rolled-up tubes. All samples were grown on top of 200 Å AlAs etchant-sensitive layers deposited on GaAs(001) substrates. For the first sample—referred to as "bilayer"—185 Å of $In_{0.2}Al_{0.2}Ga_{0.6}As$ and 185 Å of GaAs were deposited on top of the AlAs layer. In this bilayer the In mainly determines the strain while the replacement of Ga atoms by Al atoms slightly modifies the elastic constants. In the second sample, four layers were stacked on top of the AlAs film by repeating twice the deposition of a bilayer structure of 200 Å of $In_{0.2}Ga_{0.8}As$ and 300 Å of GaAs. This sample, referred to as "quadlayer," was designed to probe the possibility of nonmonotonic radial strain relaxation across the interfaces. Finally for the last sample, that we named "dislocated," a bilayer structure of 250 Å of $In_{0.33}Ga_{0.67}As$ and 250 Å of GaAs was grown. Since the critical thickness for the ternary alloy film with 33% of In atoms in the III site is smaller than 40 Å,[30] a large density of defects is expected and, therefore, a different relaxation after rolling. The layer layouts for the bilayer, quadlayer, and dislocated layers are schematically represented in the left panels of Figs. 2(a)–2(c), respectively.

The right panels of Figs. 2(a)–2(c) show x-ray reflectivity measurements performed on the corresponding reference flat layers, which are sketched in the left panels, as a function of $q_r=(4\pi/\lambda)[\sin(2\theta/2)]$, where λ is the x-ray wavelength and 2θ is the detector angle. The nominal grown layer thicknesses are compared with the values of x-ray reflectivity simulations[31] for the flat layers and (004) x-ray diffraction from the rolled-up layers in Table I. For the flat layers the differences between nominal and measured thicknesses are inside the error bars from the growth and fitting processes. The small discrepancies obtained in the rolled-up layers will be addressed further in the text for each case.

For the bilayer sample the rolled-up tubes were lithographically positioned by a two-step etching procedure. As shown in the left panel of Fig. 3(a) 200 μm stripes followed by 300 μm spacers were defined along the [100] direction. The topmost GaAs layer was then removed in the spacers by $H_3PO_4:H_2O_2:H_2O$ (1:10:500) shallow wet etching.[7] In a second photolithography step the underneath AlAs layer was laterally exposed by deep narrow trenches along the [010] direction obtained after etching in a HBr(50%):$K_2Cr_2O_7$(0.5 mol/l):CH_3COOH(100%) (2:1:1) solution.[15,32] Finally the layers were released by etching the AlAs layer with diluted HF(50%):H_2O (1:10) solution for 40 s. The resulting 200-μm-long tubes have an inner radius of 1.3 ± 0.1 μm and performed about ten rotations as shown by the SEM image of the inset of Fig. 2(a). In the shallow etched areas the film does not perform rotations and only produces wrinkles on the surface.[33] The preparation procedure employed for the bilayer was optimized for producing tubes with up to ten rotations, minimizing the occurrence of cracks along the tube, in order to explore the effect of multiple rotations in the strain profile of the layers. In the quadlayer sample, long (500 μm) deep trenches were defined lithographically to minimize tube cracks, and tubes with 14 ± 0.3 μm radius and a maximum of two windings were obtained.

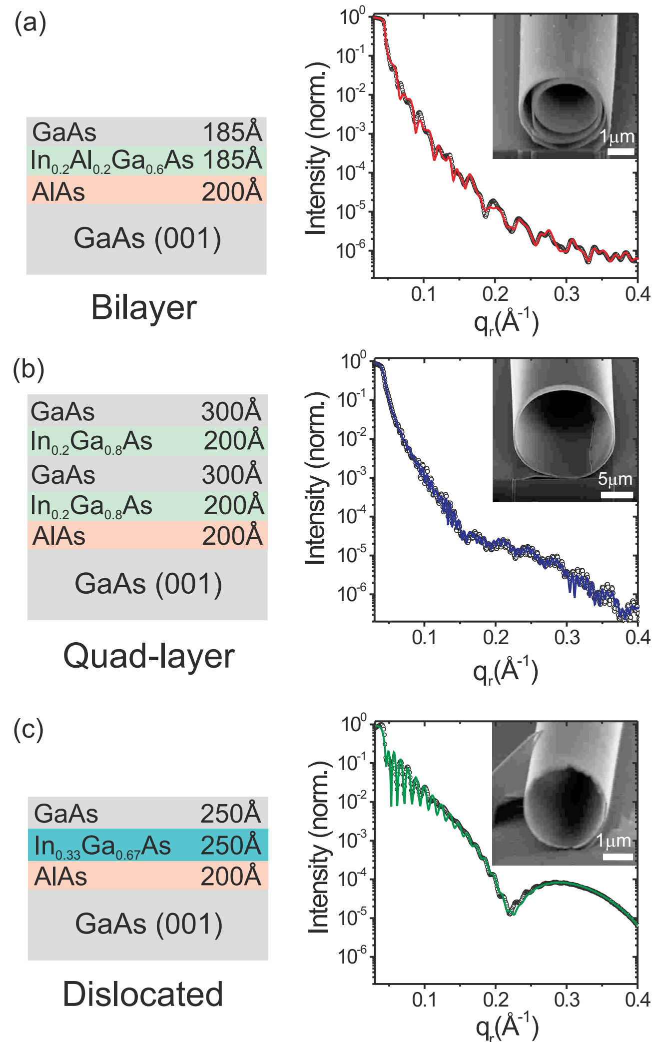

FIG. 2. (Color online) [(a)–(c)] Left panels: schematic layer layouts with nominal thickness of the samples used in this work: (a) bilayer, (b) quadlayer, and (c) dislocated layer stack. X-ray reflectivity measurements (open dots) performed to extract the thickness of each flat layer stack are shown in the right panels of (a)–(c). The solid lines in all graphs are fits using PARRATT32 (Ref. 31). SEM images of tubes obtained after rolling of the layers sketched in the left panels of (a)–(c) are shown in the insets.

Finally for the dislocated sample the trenches were obtained from surface scratching and long rolled-up tubes were produced exhibiting a radius of 1.5 ± 0.1 μm with five to six rotations. For all samples the tubes roll along one of the ⟨010⟩ directions. Tube openings are shown in the SEM images of the insets for all cases.

B. X-ray diffraction from single tubes

The x-ray microdiffraction experiments were performed at the ID01 beamline of the European Synchrotron Radiation

TABLE I. Nominal and measured layer thicknesses for the flat and rolled-up layers. Values of average roughness σ obtained from the fits of the reflectivity curves (Fig. 2) are also provided.

Sample	Layer	Nominal thickness (Å)	Reflectivity flat layer thickness (Å)	Diffraction rolled layer thickness (Å)
Bilayer	GaAs	185	198 (σ=2)	190 (σ=20)
	$In_{0.2}Al_{0.2}Ga_{0.6}As$	185	189 (σ=2)	150 (σ=20)
Quadlayer	GaAs (top/inner)	300	285 (σ=10)	280 (σ=30)
	$In_{0.2}Ga_{0.8}As$ (top/inner)	200	196 (σ=9)	190 (σ=30)
	GaAs (bottom/outer)	300	314 (σ=9)	270 (σ=30)
	$In_{0.2}Ga_{0.8}As$ (bottom/outer)	200	213 (σ=9)	180 (σ=30)
Dislocated	GaAs	250	227 (σ=40)	225 (σ=45)
	$In_{0.33}Ga_{0.67}As$	250	237 (σ=48)	230 (σ=45)

Facility (ESRF) by using Be compound refractive lenses (CRLs). The focused x-ray spot achieved at 8.8 keV (λ $=1.409$ Å) has a size of 6×6 μm^2 at the sample position and a divergence of 0.05°. Such spot size is small enough to measure diffraction from single tubes. The flux density gain after the CRL is of approximately 5000 times, allowing for measurements in very small sample volumes. Finally, the divergence is obtained by measuring the Si(004) peak width of an analyzer Si(001) crystal. Diffraction measurements are performed using an avalanche photodiode as detector. An optical microscope aiming at the center of the 4+2 circle diffractometer allows for a view of the sample surface and optical prealignment in which the longitudinal axes of the tubes are oriented perpendicularly to the x-ray beam path as represented in Fig. 3(a).

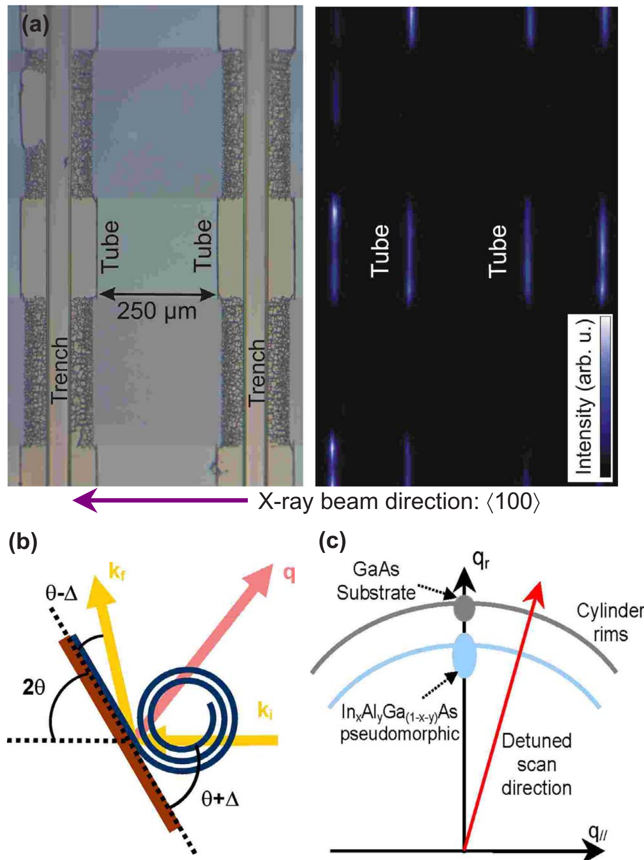

FIG. 3. (Color online) (a) Optical microscopy (left panel) and x-ray microdiffraction map (right panel) of the same region of the bilayer sample. (b) Tube diffraction geometry used for coplanar measurements detuned from the substrate lattice specular condition (Ref. 25). (c) Representation of the vicinity of the reciprocal space (004) diffraction position for flat layers (spots) and a cylindrical crystal rolled up in a tube (rims). The oblique arrow (red) in the right-side quadrant illustrates schematically the reciprocal space path of a detuned radial scan.

Diffraction measurements are then performed around the GaAs (004) reciprocal space position for all samples. The fine x-ray beam positioning on the sample can be easily performed by taking profit of the tube geometry. Since the crystalline layers inside the tubes have a radial symmetry, it is possible to suppress the diffraction from the substrate by detuning the substrate lattice from the specular θ-2θ condition as represented in Fig. 3(b).[25]

A sketch of the reciprocal space diffraction intensity distribution for the rolled-up and flat layers is shown in Fig. 3(c). While the diffraction of the flat layers consists in a much localized spot in the reciprocal space, the diffraction from the curved crystals can be observed along a powderlike rim of intensity. Hence, to enhance the sensibility on tube diffraction, a detuning is performed in the sample angle θ by adding an increment Δ of about 15° as shown in Fig. 3(b). Although the procedure can also be performed with a negative detuning, the incoming flux that illuminates the tube spreads, creating a larger footprint and therefore producing a less intense diffraction signal despite of the reduced background.

The tubes can then be found by laterally scanning the sample with the detector 2θ angle fixed at the GaAs or $In_xAl_yGa_{1-x-y}As$ (004) rolled-up layer reciprocal space position.[34] For such condition the angles define a point in reciprocal space that is sensitive to diffraction of rolled-up material solely. Consequently, a strong signal is observed when a tube is on the beam, in contrast with the absence of counts obtained from the flat film regions and shallow etched and wrinkled areas. An inspection of both panels of Fig. 3(a)

shows the correspondence between an optical image and the scanning x-ray diffraction performed in the same area of the bilayer sample.

Once a tube of interest is selected, some optimization on the alignment is required. A preliminary radial scan is performed by scanning solely the detector (2θ) angle, which allows for the observation of diffraction peaks from the layers inside the tube. The angle 2θ is then fixed to one of the peaks and the translation stages can be scanned to optimize the diffracted intensity (i.e., bring the tube into the center of the x-ray spot). Finally, it is crucial to check whether the beam is perpendicular to the tube axis by performing an azimuthal scan (hereafter referred as ϕ scan). As it will be shown in Sec. IV, ϕ scans reveal an interplay between layer size, tilting of the layers inside the tube and, therefore, the packing quality of successive windings.

IV. RESULTS AND DISCUSSION

A. Measurement and azimuthal alignment

Radial scans performed in a rolled-up tube of the bilayer sample and on the reference flat layers are shown in Fig. 4. Both scans were performed in the vicinity of the GaAs (004) reflection and their corresponding paths in reciprocal space are represented in Fig. 3(c). The inset of Fig. 4 shows a schematic of the sections in a rolled-up tube that contribute to diffraction at the (004) position. The main contribution comes from the two opposite sectors in which the radial lattice planes are oriented perpendicularly to the momentum-transfer vector.[25] Hence, in a detuned radial scan the radial lattice-parameter profile is measured along the ⟨004⟩ direction. It is possible to draw preliminary qualitative conclusions by simple inspection of both measurements. In the flat system the GaAs layer is completely unstrained while the $In_{0.2}Al_{0.2}Ga_{0.6}As$ layer is under a biaxial compressive strain $\varepsilon_{\parallel}$ imposed by the host GaAs(001) substrate. An out-of-plane expansion given by $\varepsilon_z=-2(C_{12}/C_{11})\varepsilon_{\parallel}$ is then observed for this In-rich layer ($\varepsilon_{\parallel}=\varepsilon_x=\varepsilon_y$ for the flat film), leading to an out-of-plane lattice parameter of 5.822(2) Å. Such value, obtained from the $In_{0.2}Al_{0.2}Ga_{0.6}As$ peak position, is in agreement with the nominal composition of the pseudomorphically strained layer.[35] Curving the layers into a tube will allow for a partial in-plane relaxation of the $In_{0.2}Al_{0.2}Ga_{0.6}As$ film along the tangential direction as depicted in Fig. 1(b), leading to an out-of-plane—radial for the curved layers—contraction for a fixed ε_l. As a result, the diffraction peak for the rolled-up layer shifts to larger q_r values with respect to the corresponding position for the flat layer. On the other hand, since a tangential expansion is expected along the tube wall for the given $a_l=a_{GaAs}$, the out-of-plane GaAs layer lattice also contracts slightly. Therefore, the corresponding lattice-parameter difference between the two layers decreases, which is observed as an approaching of the two peaks in Fig. 4.

Prior to a detailed interpretation of the measurements and introduction of an x-ray model, some comments should be made concerning the reciprocal space profiles observed by performing an azimuthal tube alignment. Considering the beam divergence of 0.05°, the tangential section of a tube where the lattice is aligned perpendicularly to the momentum-transfer vector has a much reduced dimension of about 10 Å. Since the beam spreads laterally along its 6 μm size, the useful footprint for diffraction is about 0.006 μm^2 as represented in Fig. 5(a). Such dimensions are consistent with relative diffraction intensities calculated with respect to the incoming flux and the diffraction from flat layers and make the use of a focused beam mandatory for recording reasonable signals. For the footprint geometry shown in Fig. 5(a), the ϕ-dependent diffraction width is related to three factors: (i) the tube radius R_i, which implies that in small diameter tubes with pronounced curvatures the diffracted intensity should be more sensitive to the ϕ alignment (narrower profile); (ii) the folding faults and tilting of neighbor windings, which would produce a mosaic spread of scattering due to imperfections in the matching of internal walls. A larger number of these faults would then be proportional to the number of windings w; (iii) the size broadening due to the finite layer thickness.

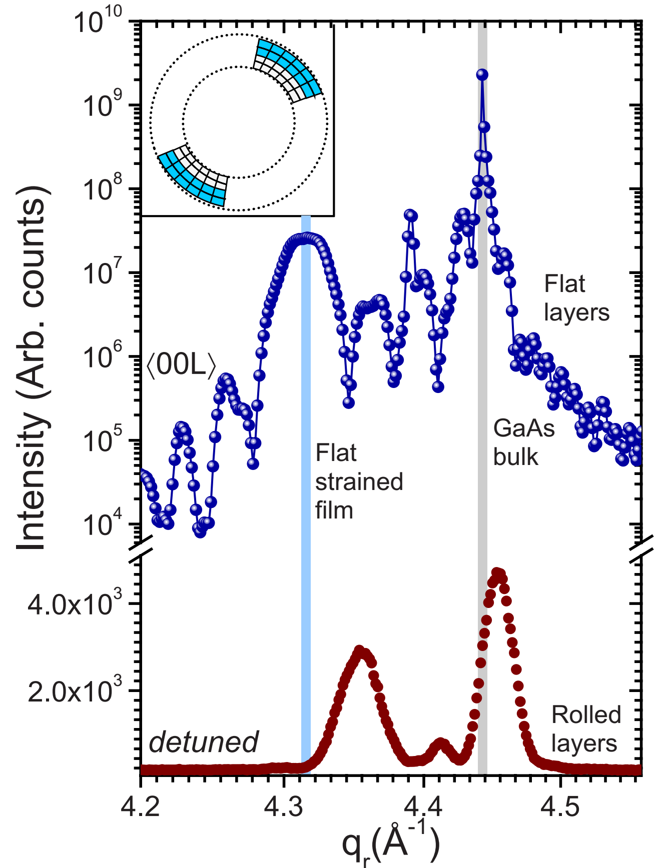

FIG. 4. (Color online) Radial scans in the vicinity of the GaAs(004) reflection for the flat bilayer sample (blue dots, upper curve) and the rolled-up layers (red dots, lower curve). The blue line used for the flat layer data is a guide for the eyes (just connect dots). The partial strain relaxation that takes place after rolling can be observed as a shift in reciprocal space of the peaks in the red dot curve with respect to the GaAs bulk and pseudomorphically strained $In_{0.2}Al_{0.2}Ga_{0.6}As$ film positions. The inset shows schematically radially opposed regions of the tube that contribute to the x-ray diffraction signal (Ref. 25).

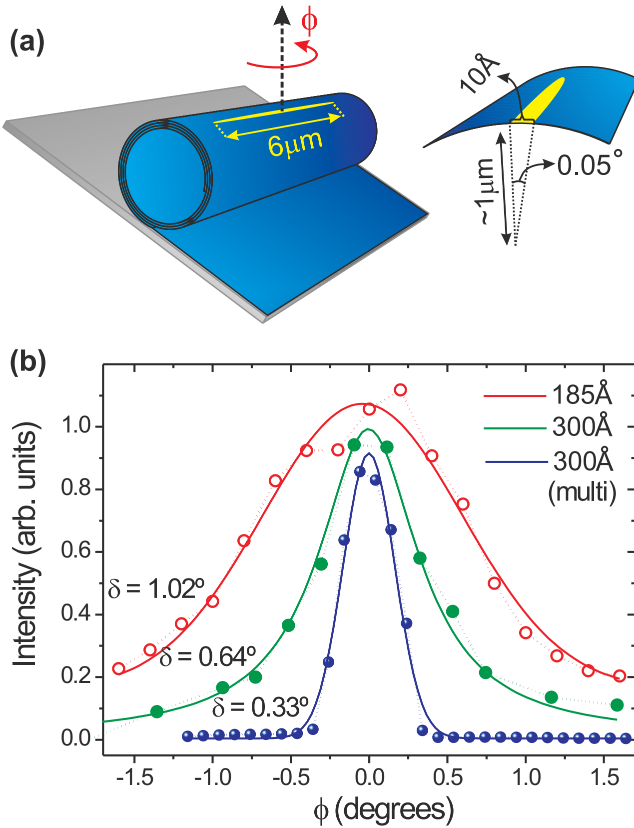

FIG. 5. (Color online) (a) Representation of the x-ray diffracted beam footprint and the geometry of ϕ scans. (b) ϕ scans performed at the detuned GaAs (004) peak position for three tubes with different layer thickness. The red and green lines are Lorentzian fits to scans in a 185 (red open dots) and 300 Å (green solid dots) GaAs layers in bilayer tubes, respectively. A similar scan with corresponding fit in the quadlayer tube (blue solid dots/line, narrowest profile) is also shown.

Figure 5(b) shows ϕ scans obtained at the fixed reciprocal space position for the tube GaAs peak of Fig. 3 in tubes with different total layer thickness. For GaAs layers with 185 Å and 300 Å thicknesses (the last not further explored here) embedded in bilayer, tubes with a large number of rotations—ten and seven, respectively—and inner radius of 1.5 μm and 2 μm are obtained, respectively. The peak of the 300 Å GaAs layers of a quadlayer tube—with an inner radius of 7 μm and only one layer turn—is also shown. Although the exact interplay between folding and tilting mosaics and the tube radius cannot be directly evaluated from the widths of these curves, one can infer an upper bound of the effective overall mosaic spread for the layers, which includes the previous factors, by deconvoluting the angular width of these curves with their expected size broadenings. In such approach the effect of the radius R_i is assumed as considerably smaller than the mosaic/tilt induced broadening.

For the given diffraction geometry the calculated thickness-dependent angular width $\Delta\phi$ is given by $\Delta\phi = a \sin(2\pi/q_r d)$, where a is the local lattice parameter, d is the GaAs or $In_xAl_yGa_{1-x-y}As$ layer thickness, and q_r is the reciprocal space position of the layer diffraction peak. For our tubes $\Delta\phi = 0.436°$ for the GaAs 185 Å thick layer while the GaAs 300 Å thick layer has $\Delta\phi = 0.269°$. The overall layer mosaic spread M for the three tubes shown in Fig. 5(b) can then be calculated as $M = (\delta^2 - \Delta\phi^2)^{1/2}$,[36] where δ is the measured angular width of a ϕ scan. For the larger profile of the 185 Å layer $M = 0.92°$ was obtained. This value is slightly larger than the value obtained on the 300 Å bilayer tube, with $M = 0.58°$, and much larger than M for the 300 Å quadlayer tube, which exhibits $M = 0.19°$. In all cases discussed above the beam divergence is much smaller than the obtained mosaic spread values.

A comparison of M values for these three tubes indicates that there is a stronger dependence on the overall layer mosaic spread on folding and tilting faults [factor (ii) described above] than on the tube radius. A multirotation tube formed from a thinner— and therefore fragile—layer is susceptible to develop more layer tilts or loosely packed windings with respect to a tube made of thicker layers. Such behavior is indicated by the narrow ϕ-scan profile measured in the 1000 Å wall thickness (300 Å multilayer) of the quadlayer tube. Despite exhibiting a much larger tube radius (7 μm), which would induce a broader profile according to the geometrical factor (i), such thicker tube wall is quite robust against tilting and folding faults. Scans in ϕ performed at the $In_{0.2}Ga_{0.8}As$ peak of the quadlayer tube have shown identical profiles. Hence, a ϕ alignment is always needed to optimize the diffracted intensity by tuning the preferred packing orientation of the tube windings and reveals quantitative information on the average mosaic spread of the layers.

B. X-ray model and fit precision

In order to quantitatively analyze the diffraction from the tubes produced from the layer systems of Fig. 2, one must introduce a convenient x-ray model. Such model will be based on four assumptions: (i) The reduced layer thickness allows for the use of kinematical theory; (ii) the diffracted intensity is mainly sensitive to the scattering from a region of the tube where the radial lattice parameter is aligned to the momentum-transfer vector, and, therefore, probes mainly the a_r lattice profile; (iii) the total diffraction intensity measured is an incoherent sum of the intensities of all W turns due to the random crystal misalignment between successive windings and the formation of a thin oxide layer at the interfaces;[19] (iv) the tube is homogeneous along its longitudinal direction on a length scale of the order of the x-ray beam size (6 μm) which is used to probe its properties.

The q-dependent diffraction intensity observed from a multirotation tube will then be given by

$$I(q) = I_0 \sum_{w=0}^{W-1} \left| \sum_{n=0}^{N-1} \left(\sum_{j=0}^{A_n} f_n e^{iqr_j} e^{-q(\sigma^2/2)} \right) \right|^2, \quad (6)$$

where the summation over w accounts for the incoherent diffraction of the successive windings, the summation over n accounts for the layer stack in each wall, and the summation over j accounts for the atom positions in each layer r_j along the tube radial direction.[37] In this equation f_n and A_n are the average effective atomic scattering factor and the number of

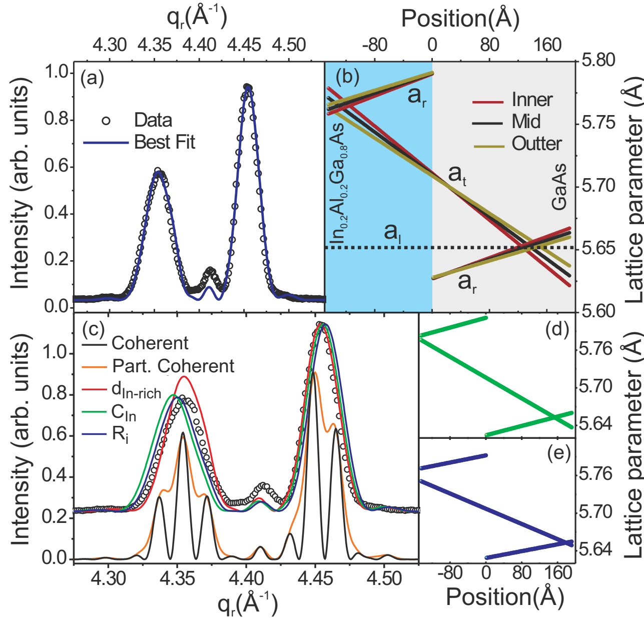

FIG. 6. (Color online) (a) Radial scan measurement (dots) and simulation (line) for the bilayer tube. (b) Lattice-parameter profiles in the inner, outer, and middle layers of the ten turn tube simulation used to fit the data of (a). (c) Fits using nonoptimal parameters, used to extract effective intrinsic error bars of the modeling and infer the fit precision (see text for detailed explanation). (d) Lattice-parameter profile for an In concentration of 0.21 in the In-rich layer. (e) Simulated lattice-parameter profile for a value of R_i 10% larger than the equilibrium value. The solid green and blue lines in (c) correspond to simulated diffraction profiles from (d) and (e).

atoms in the layer n, respectively. For the rolled-up tubes σ represents an effective overall roughness, which takes into account also the changes in the position of the interfaces in the x-ray illuminated area due to the original flat layer roughness as well as due to the local tube tangential curvature and the longitudinal waviness of the layers. The input parameters for a calculation of the diffraction curve using Eq. (6) are σ, f_n, and the atomic positions. These later are obtained by the following procedure. First the constants R_i and a_i are extracted by minimizing the elastic energy for the first turn. Then, using Eq. (2) the tangential lattice profile is obtained for all positions inside this layer stack. The radial lattice-parameter (a_r) profile as a function of the position in the tube is then generated by applying Eq. (3). Similar a_r profiles are also obtained for $R_w=R_i+wD$, where D is the total layer stack thickness ($D=\Sigma\Delta d_n$). Finally, the calculated atomic positions are used as input for Eq. (6) and a simulation of the diffraction profile is obtained.

Figure 6(a) shows the best fit found for the data recorded on the bilayer sample. This fit was obtained for an $In_{0.2}Al_{0.2}Ga_{0.6}As$(150 Å)/GaAs (190 Å) bilayer with $R=1.30$ μm, σ=20 Å, $a_l=a_{GaAs}$ (no longitudinal relaxation), and the nominal In and Al concentrations. Identical diffraction profiles were found in different tubes rolled up from the same sample. The reduced layer thickness obtained in the diffraction simulation is attributed to a thin oxide formation after the layer release, as discussed in Ref. 38. Particularly for the $In_{0.2}Al_{0.2}Ga_{0.6}As$ layer, a more pronounced difference with respect to the nominal and measured flat layer thickness shown in Table I is obtained. Nevertheless, assuming the formation of a native oxide with maximum thickness of 20 Å for the Al-rich layer, the deviations from the thickness obtained from different methods lie inside the estimated error bars. Corresponding lattice-parameter profiles for the inner, middle, and outer windings for ten turn tubes are shown in Fig. 6(b). The fixed longitudinal lattice parameter [dashed line in Fig. 6(b)] indicates that no relaxation takes place in this direction during rolling or after it, evidencing that a strong waferlike layer bond takes place between adjacent windings.

The fitting values used for the bilayer tube indicate a very good agreement with the continuum elastic theory as also shown in other tubes explored in Ref. 25. It is worth probing the actual error bars on the fitting procedure and its dependence on each of the modeling parameters. This is shown schematically in Fig. 6(c). Although Eqs. (2)–(5) interconnect the values of the fitting variables R_i, a_i, ε's, and a's, we depict the effect of changing independently one parameter in the fit while keeping the others fixed in their optimized value. Such procedure establishes, semiquantitatively, intrinsic error bars of the x-ray diffraction modeling. For the bilayer the most relevant parameters are: (i) $In_{0.2}Al_{0.2}Ga_{0.6}As$/GaAs layer thickness; (ii) In concentration (C_{In})—here we assume that the Al influence on strain is negligible for the concentration used; (iii) longitudinal lattice parameter a_l (or alternatively the longitudinal strain ε_l); and (iv) tube inner radius R_i.

Maybe the most evident parameter is the layer thickness ratio of item (i). An incorrect balance between d_{GaAs} and $d_{InAlGaAs}$ renders the intensity of one peak larger than the other, as shown by the red curve of Fig. 6(c). Additionally, an error in the total thickness changes the strain distribution and, therefore, the position of the peaks in q, which drift in opposite directions. From the fitting procedure it is possible to estimate the error bar for this parameter as small as 15 Å.

A change in the In concentration—item (ii)—will displace both peak positions laterally in opposite q directions as shown by the green curve due to a change in strain. Figure 6(d) depicts the changes observed in the lattice-parameter profile by increasing the In concentration C_{In} by 1%. The effective error bar for C_{In} was found to be about 0.5%. The Al content (C_{Al}) was also varied in our simulations (not shown). Although it introduces no strain the presence of Al atoms in the layer alters its elastic properties. C_{Al} has proven to effectively change the fit quality only for a concentration that differs from the nominal by more than 10%.

Changing a_l (or ε_l)—item (iii) will move both peaks laterally on the q axis in the same direction. In the case $a_l > a_{GaAs}$ the longitudinal expansion of the lattice parameter will produce a contraction in a_r for the GaAs layer. For the In-rich layer a contraction in a_r is also observed and therefore both peaks are shifted to higher values of q. An effective error bar of $\Delta\varepsilon_l \cong 0.08$ was found. Changes in this condition will be further explored while fitting the quadlayer and dislocated tubes (Secs. IV C and IV D, respectively).

Finally it is worth analyzing the effect of a change in R_i. As shown by the blue curve of Fig. 6(c) and the lattice-parameter profile in Fig. 6(e), a 10% larger value of R_i will

split the peaks apart while smaller R_i values will bring them closer. For the given bilayer tube the fit is sensitive to variations in R_i of about 4%. Here one must notice that, as shown in Fig. 5(a), the x-ray diffraction method probes a much reduced volume of the rolled-up crystalline layers. The value of R_i obtained by this method represents the local curvature of the illuminated tube area. However, by measuring several tubes and/or several positions along one tube, it is possible to average the diffraction profile and extract a realistic R_i. In round and well-packed tubes like the ones used in this work, radial scans performed in different positions or different tubes are very similar. Finally, the values of R_i obtained by all fits are in very good agreement with direct methods such as SEM and TEM, showing that local curvature and radius coincide for our structures.

A quick exploration on the effect of the incoherent sum given by Eq. (6) is also performed. The lower solid black line in Fig. 6(c) corresponds to the expected diffraction profile for a completely coherent lattice matching in each two turns in the bilayer tube. For such system the summation in w (windings) of Eq. (6) is set inside the squared modulus. The result is a curve with discrete peaks separated by the reciprocal of the bilayer thickness ($2\pi/D$) with an external envelope given by the fully incoherent fit of Fig. 6(a). A more realistic situation where the lattices of only two of the windings are coherently matched and all other turns interfere incoherently is represented by the orange solid line of Fig. 6(c). Although a completely crystalline bonding through the whole rotation is unexpected, this situation would represent a tube where a considerable amount of large aligned crystalline bonded areas can be found. Considering the effects of roughness and beam divergence, the interference minima of the wiggling would be less pronounced although still measurable. No evidence of coherent layer matching in large areas between neighboring windings was found for any of the tubes that were measured, as well as for the tubes from Ref. 25. This can be explained by the imperfect crystal lattice matching in the interfaces of windings as well as by the formation of a thin amorphous oxide layer.[38]

C. Multilayer tube

The degree of partial strain relaxation that takes place after the rolling process is strongly dependent on the layer stack. While for bilayer tubes the resulting strain profile after roll indicates a good agreement with the continuum elasticity description employed in the last session, it is worth understanding whether such model may be also applied in a system where a nonmonotonic relaxation takes place. Figure 7(a) shows a radial scan performed in the flat reference layers for the quadlayer sample. The larger number of minima and maxima with respect to the bilayer flat films of Fig. 4 is generated by the double repetition of the 300 Å GaAs/200 Å $In_{0.2}Ga_{0.8}As$ stack. As observed for the bilayer sample, the peak of the In-rich layer indicates an out-of-plane lattice parameter of 5.820(2) Å (q_r =4.318 Å^{-1}), expected for a 1.4% in-plane strained film with the nominal 0.2 In content.

A radial scan on the rolled-up tube is shown in Fig. 7(b). Despite the curvature of the surface, the measured profile

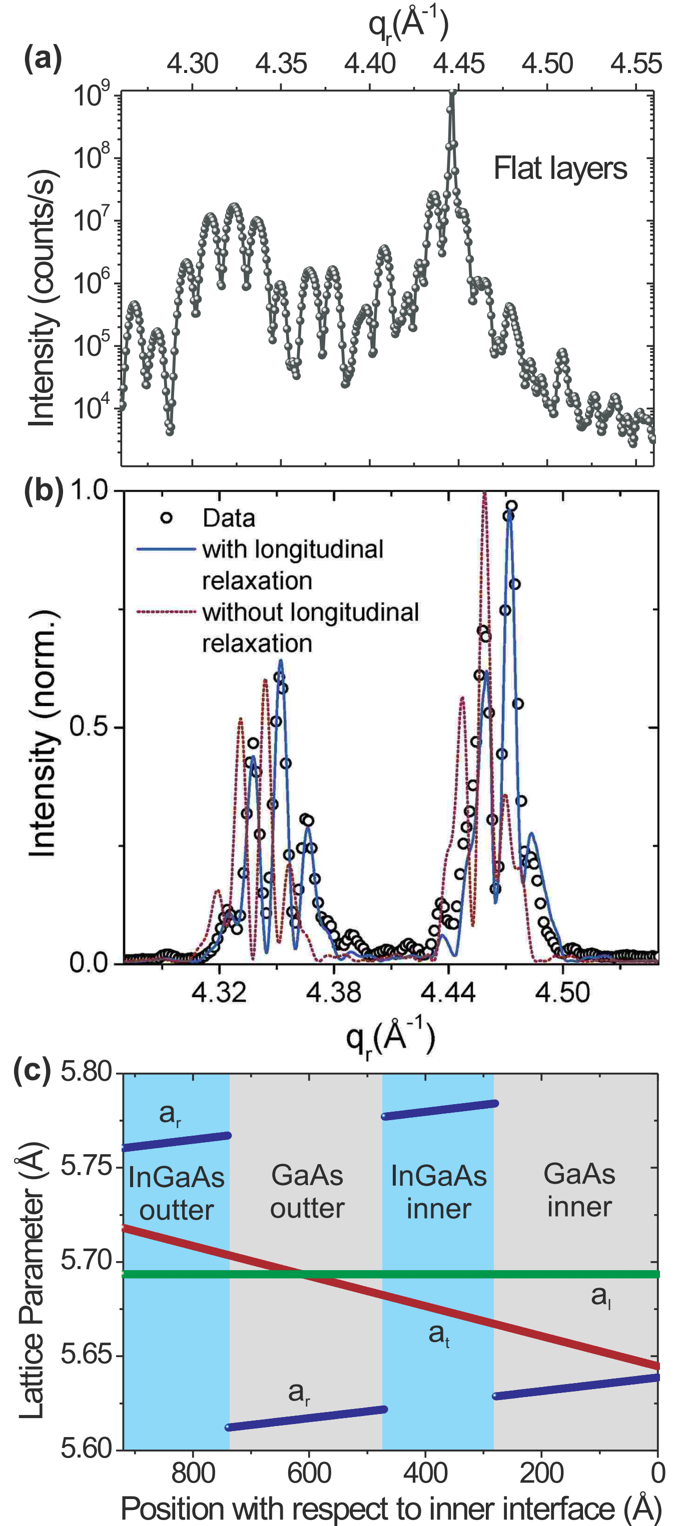

FIG. 7. (Color online) (a) Radial scan near the GaAs(004) reciprocal space position for the quadlayer sample. The line is a guide for the eyes. (b) Radial scan (open dots) in a rolled-up tube from the quadlayer system. The dashed red curve represents a fit without longitudinal lattice-parameter relaxation. For the blue solid line a relaxation of the lattice along the tube axis of 0.7% is assumed. (c) Lattice-parameter profile for the quadlayer obtained from the best fit of (b).

(open dots) exhibits several deep sharp minima as for the flat layers, indicating that the layers scatter as much softly bowed structures due to the small extension of the beam tangential footprint. A first attempt to simulate the observed x-ray profile is shown by the red dashed line. Assuming that no relaxation takes place along the longitudinal direction of the tube, one cannot reproduce the exact peak position and/or their relative intensities. Since the tube radius, calculated[22] and also observed as 7 μm, is much larger than in the bilayer case, the wafer bonding between successive windings will only occur after a long extension of flat material has been already relieved from the substrate constraints. The much larger perimeter of the cylinder implies a reduced influence of the unetched film in the final tube strain status. It is, therefore, reasonable to assume that some longitudinal relaxation occurs. In fact, the best fit of the diffraction profile can only be obtained by fixing a longitudinal lattice parameter intermediate between the GaAs and $In_{0.2}Ga_{0.8}As$ bulk values [shown in Fig. 7(c)]. Such value corresponds to a longitudinal strain of 0.7%, compressive for the In-rich layers and tensile for the GaAs layers. By assuming the longitudinal strain above, the external envelope of the curves shifts into the larger q_r direction, and a more suitable balance between the sharp peak intensities is found. This shift of the fit curve cannot be obtained by changing any other parameter in the simulation. An effective error bar for the longitudinal strain determination can be estimated as $\pm 0.2\%$ for this case.

The layer thicknesses used in the simulations of Fig. 7(b) for the GaAs inner and outer layer are 280 Å and 270 Å, respectively. For the $In_{0.2}Ga_{0.8}As$ layers we have obtained 190 Å (inner layer) and 180 Å (outer layer). The tube radius found by the minimization of the elastic energy given by Eq. (4) was $R_i = 6.94$ μm, in agreement with the value found using the evaluation method of Ref. 22 (6.88 μm). An average roughness $\sigma = 30$ Å was used for the fitting.

Figure 7(c) shows the lattice-parameter profile obtained from the fit of Fig. 7(b). By a simple inspection of the less pronounced slopes of tangential and radial lattice-parameter profiles, it is possible to infer that the releasing of the elastic energy in this tube by rolling is much less effective than in the bilayer tube. However, the longitudinal lattice-parameter relaxation adds another degree of freedom for the energy minimization, leading to a structure where the final local stored elastic energy is similar to the bilayer case. A more quantitative and detailed discussion will be done in Sec. IV E.

D. Dislocated layer tube and effective strain

A limiting case for the use of the continuum elastic model shown would be a tube in which one or more layers have a large density of defects. For such tubes the possibility of rolling as a strain releasing process is still possible.[39] The tube rolling can be used, then, to probe the effective strains which are stored in these layers.[40] The dislocated layer rolled here is obtained from a $In_{0.33}Ga_{0.67}As$/GaAs bilayer in which the In-rich film thickness (~250 Å) is much larger than the critical thickness for this given concentration [~40 Å (see Ref. 30)]. A density of edge dislocation defects of about $10^6 - 10^7$ cm^{-2} is expected.[41]

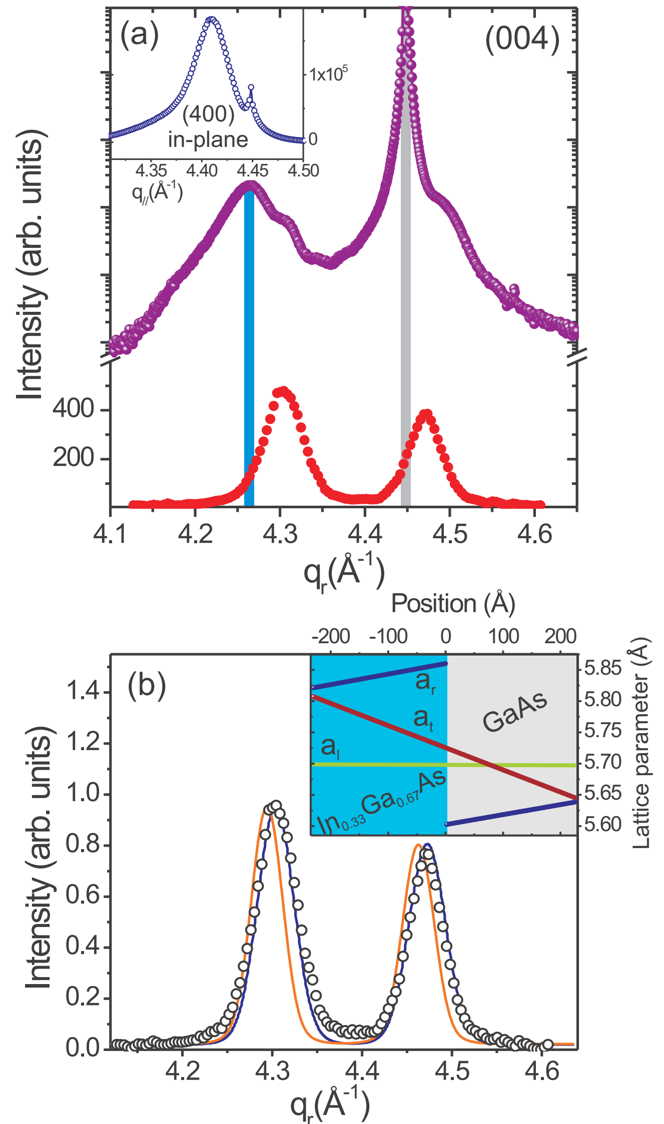

FIG. 8. (Color online) (a) Radial scans in the vicinity of the GaAs (004) reflection for the flat and rolled-up dislocated layers. The inset shows a grazing-incidence radial scan close to the (400) in-plane reflection, allowing for the determination of the lattice parameter of the flat layers in the plane of the substrate. (b) Measured radial scan (dots) and fits to the dislocated tube diffraction. The orange solid line is obtained for the condition $a_l = a_{GaAs}$ while the blue line is the best fit assuming a 0.7% longitudinal lattice relaxation. The inset shows the lattice-parameter profile that corresponds to the best fit.

Figure 8(a) shows the measured diffraction intensity in the vicinity of the GaAs (004) reciprocal space position for the flat and rolled-up dislocated tube layers. A quick comparison of the radial scan in the dislocated flat film and the scan performed in the defect-free bilayer sample of Fig. 4 evidences a considerably larger roughness of the first.[39] Despite the large number of dislocations the $In_{0.33}Ga_{0.67}As$ peak position for the flat layer [$a_\perp = 5.899(2)$ Å] corresponds to a pseudomorphically strained InGaAs alloy with 30% In content, indicating that only a reduced fraction of the 2.2% in-plane strain is released by defect formation. A radial scan

performed in grazing-incidence geometry directly shows an in-plane average lattice parameter of 5.695(2) Å for the dislocated bilayer. Such value corresponds to a relaxation of 0.7% with respect to a hypothetical coherent biaxially strained $In_{0.33}Ga_{0.67}As$ film on GaAs.

Two fits of the dislocated tube diffraction are shown in Fig. 8(b). Particularly in this case, in which plastic deformations take place, the use of nominal parameters of layer thickness and strain, assuming a defect-free tube, leads to an extremely different lattice-parameter distribution inside the rolled-up layers and is unable to model the observed diffraction profile. By employing the energy minimization method described in Sec. II, as well as the solutions proposed by Refs. 22 and 28, one obtains a tube radius of 1 μm, much smaller than the observed 1.5 μm. Alternatively, for the layer configuration of 250 Å $In_{0.33}Ga_{0.67}As$/250 Å GaAs, a tube with the observed 1.5 μm radius can only be obtained from the methods of Sec. II by assuming an In content of 0.22 and the corresponding strain of 1.5% given by such concentration. Such value corresponds directly to the 0.7% relaxation obtained in the in-plane (400) diffraction. Therefore, the observed radius of a tube with dislocated layers provides already a fairly good estimation of the amount of strain, which is released by the formation of defects.

By fixing the radius $R=1.5$ μm in Eq. (4) a reasonable lattice-parameter configuration can be found. However, although the use of the observed radius accounts in part for the strain released during layer deposition, an In content of 0.33 must be used to generate the correct lattice-parameter profile which fits the tube diffraction. This finding can be explained by the dimensions of the diffracted beam footprint, discussed in Sec. IV A. For the dislocation densities expected here, only one or two defects per bilayer turn will be illuminated in the 0.006 μm^2 effective diffraction area. Therefore, the local effects of the strain induced due to the In-rich alloy will prevail over the presence of dislocations. In other words, such result also suggests that the volume of material in the layers affected by the presence of dislocations is about two orders of magnitude smaller than the volume which remains unaffected by the defect strain field and is probed by the x-ray beam. The orange solid line of Fig. 8(b) is then obtained by minimizing Eq. (4) for a 230 Å $In_{0.33}Ga_{0.67}As$/225 Å GaAs bilayer, with fixed $R_i=1.5$ μm, $C_{In}=0.33$, and $\sigma=45$ Å.

Finally, a longitudinal lattice parameter of $a_l=5.70$ Å must be used in Eq. (4) in order to bring the simulated peaks into the correct q_r positions as represented by the blue solid line of Fig. 8(b). The use of this value corroborates the initial strain status of the layers and indicates that, as for the bilayer sample of Sec. IV B, an interlayer waferlike bonding in small radius tubes keeps the longitudinal strain status of the flat films. The final lattice-parameter profile obtained is shown in the inset of Fig. 8(b).

Although a direct and quantitative comparison between strain relaxation via defect formation and due to layer bending/rolling cannot be drawn, the influence of each process in the tube formation can be understood as follows. Edge misfit dislocations in the In-rich layers of III-V tubes will relieve the strain in an inhomogeneous way, with a more effective relaxation taking place at the vicinity of the defects. Bending the layer is, in contrast, a homogeneous relaxation process in which the average per-atom strain reduction adds over the whole layer volume. Qualitatively it is possible to probe the practical threshold of the interplay between (i) relaxation by bending and (ii) defects by rolling up layers with different defect densities, and, therefore, different effective strains.[41] The relief of strain, ultimately depicted by the elastic energy profile inside the rolled layers is explored quantitatively in Sec. IV E.

E. Local elastic energy and partial relaxation

Although the relaxation of the longitudinal lattice of two of the tubes presented here accounts for a small change in the radial lattice-parameter profile and, therefore, the observed tube diffraction, it strongly influences the final elastic energy stored inside the rolled-up layers. It is worth, therefore, to understand how the elastic energy varies locally inside the tube walls.

Applying Eq. (1) to the lattice-parameter profile of the bilayer tube shown in Fig. 6(b) leads to the elastic energy profile of Fig. 9(a). The energy stored in the flat pseudomorphically strained $In_{0.2}Al_{0.2}Ga_{0.6}As$ film, represented by the black horizontal line, is partially released during roll. In the flat layers the In-rich film stores a per-atom energy of 3.28 meV while the total energy in the bilayer, evaluated for an atomic chain perpendicular to the surface, is of 353 meV. After the rolling of the layers, part of the initial energy is redistributed between the GaAs and the In-rich layers while another part is released in the rolling process. Although after the formation of the tube most of the energy (~85%) remains in the In-rich film due to the absence of longitudinal relaxation in this tube, a small fraction of about 15% of the total final energy is stored in the GaAs layer. The energy difference between the inner and outer layers, also shown in Fig. 9(a), is very small. While the radially integrated energy for an atomic chain of the inner winding is equal to 160 meV, it reaches 164 meV after ten turns. Despite such difference of about 2.5% the positions of the energy minima of each layer shift outward as the number of turns increases. The comparison of integrated elastic energies along atomic chains discussed here for the flat and rolled-up layers provides an estimation of the magnitude of the elastic driving forces involved on the rolling process. This is represented by the energy difference between the flat and rolled-up cases.

In the quadlayer a more complex energy redistribution is found. The initial energy of 3.48 meV/atom stored in the In-rich flat layers will be shared differently with respect to their positions inside the tube wall. While the relaxation is more effective in the outer layer, the energy reduction in the inner In-rich layer is less pronounced. A similar trend is found in the GaAs layers, with the innermost layer of the tube less energetic than the one sandwiched between $In_{0.2}Ga_{0.8}As$ layers. The comparison between the red profile and the blue profile in Fig. 9(b) shows how the lattice relaxation along the tube longitudinal axis is relevant for the overall energy minimization. The local decrease in energy in the In-rich layers is enough to compensate the increment that takes place in the GaAs layers. A more equitable energy

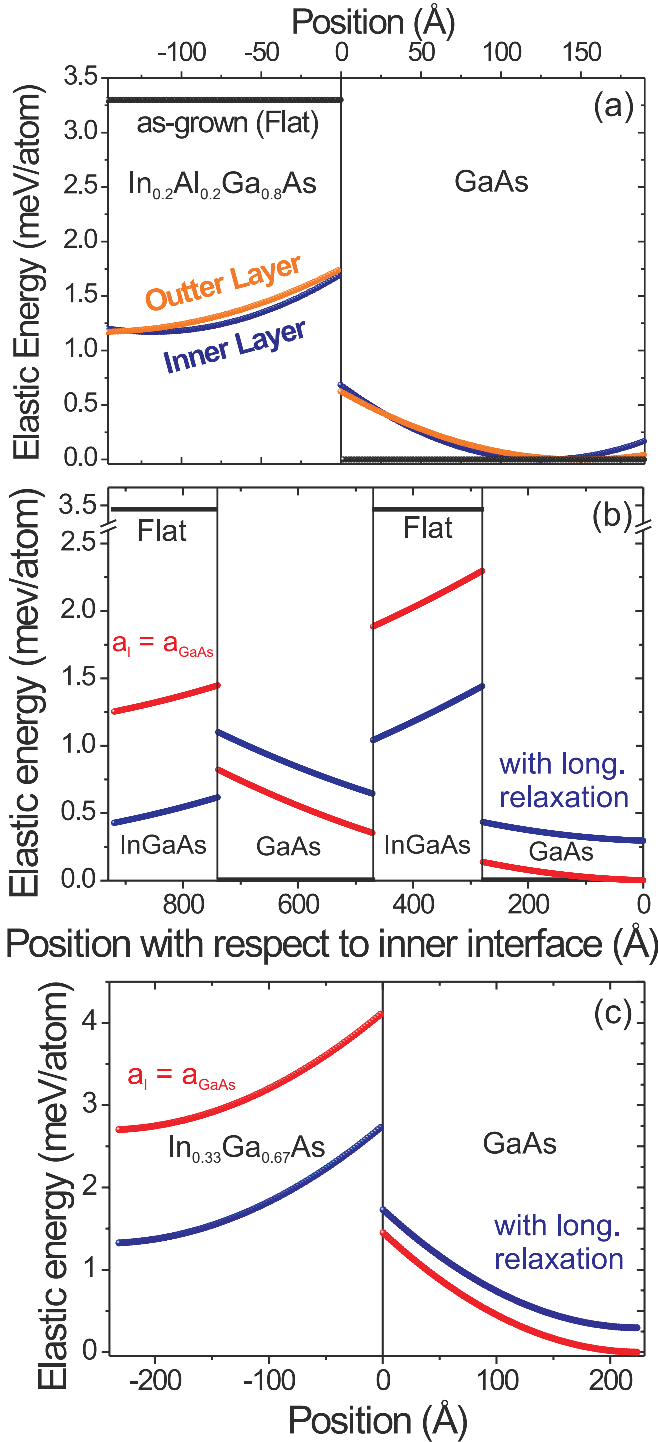

FIG. 9. (Color online) (a) Local per-atom elastic energy profiles for the as-grown (black line) and rolled-up layers of the bilayer sample. The blue line represents the local elastic energy in the inner turn while the orange line represents the outer winding for a ten-turn tube. (b) Local elastic energy for the quadlayer flat films (black line), and rolled-up tube assuming no longitudinal lattice-parameter relaxation (red lines) and the obtained lattice profile including the longitudinal relaxation given in Fig. 7(c) (blue lines). (c) Elastic energy evaluated locally for the dislocated bilayer tube, assuming $a_l = a_{GaAs}$ (red curve) and the 0.7% longitudinal relaxation (blue curve).

partition is found in this configuration, with about 50% of the final elastic energy stored in both GaAs layers, which account nevertheless for 2/3 of the wall volume, and 50% in both $In_{0.2}Ga_{0.8}As$ inner and outer layers. The integrated energy along a radial atomic chain reduces from 568 meV for the configuration with $a_l = a_{GaAs}$ to 460 meV (for the flat films $E_{chain} = 903$ meV).

Finally, the same effect of energy reduction due to longitudinal relaxation is observed for the dislocated layers. Considering the limit case of dislocated free films for this sample, the vertically integrated elastic energy in one atomic chain of the flat $In_{0.33}Ga_{0.67}As$ film would be of 1290 meV (8.1 meV/atom). Using the 0.7% biaxial in-plane relaxation which is suggested by the tube radius and in-plane/longitudinal lattice parameter, such value would decrease to 580 meV (3.6 meV/atom), which can be considered as a lower bound for the total dislocated bilayer elastic energy since locally the upper GaAs layer would have a tensile strain due to the partial relaxation of the In-rich film. Although it is hard to determine precisely the exact strain status of the flat layers, Fig. 9(c) shows the energetic reduction due to the partially relaxed longitudinal lattice parameter in the dislocated tube. For the obtained strain profile and observed radius of the rolled-up structure, the radially integrated energy is of 418 meV while a much larger amount (596 meV) would be expected for $a_l = a_{GaAs}$.

V. CONCLUSION

In this work we have shown how the strain distribution inside rolled-up tubes can be retrieved by x-ray microdiffraction. Additionally, ϕ scans are able to reveal the overall mosaic spread of the tube layers. A simple x-ray kinematical model allows for a quantitative fitting of the diffraction curves. The unambiguous determination of values such as layer thickness, roughness, lattice-parameter profiles, and tube diameter can be performed due to the interconnected relations of continuum elasticity represented by Eqs. (2)–(5). Radial lattice-parameter profiles directly obtained from the x-ray diffraction allow for the determination of elastic deformation of the unit cell in rolled-up layers with an inherent precision of 10^{-3} Å. From the fairly good model sensitivity to the longitudinal strain status shown here, it was possible to infer that waferlike interlayer bonding takes place in small radius tubes as shown for the bilayer and dislocated samples. In wide radius structures, such as the quadlayer tubes, the large distance from the rolled-up material to the unetched front allows for a reduction in the elastic energy via longitudinal lattice relaxation. A precise knowledge of such elastic behavior on rolled-up layers with thicknesses of few tenths of nanometers is crucial realizing strain engineering for devices based on the rolling-up principle.[10,12]

ACKNOWLEDGMENTS

The authors acknowledge H. Djazouli, M. Weisser, and E. Coric for technical support. C.D. thanks the ID01 staff for their hospitality during the beamtime measurements. This research was supported by the BMBF (Project No. 03X5518).

*Present address: Laboratório Nacional de Luz Síncrotron C.P. 6192–Campinas, Brazil. amalachias@lnls.br

[1] Y. G. Sun, W. M. Choi, H. Q. Jiang, Y. G. Y. Huang, and J. A. Rogers, Nat. Nanotechnol. **1**, 201 (2006).
[2] O. G. Schmidt, N. Schmarje, C. Deneke, C. Müller, and N.-Y. Jin-Phillipp, Adv. Mater. (Weinheim, Ger.) **13**, 756 (2001).
[3] P. O. Vaccaro, K. Kubota, and T. Aida, Appl. Phys. Lett. **78**, 2852 (2001).
[4] V. Ya. Prinz, V. A. Seleznev, A. K. Gutakovsky, A. V. Chekhovskiy, V. V. Preobrazhenskii, M. A. Putyato, and T. A. Gavrilova, Physica E (Amsterdam) **6**, 828 (2000).
[5] O. G. Schmidt and K. Eberl, Nature (London) **410**, 168 (2001).
[6] M. Hosoda, Y. Kishimoto, M. Sato, S. Nashima, K. Kubota, S. Saravanan, P. O. Vaccaro, T. Aida, and N. Othani, Appl. Phys. Lett. **83**, 1017 (2003).
[7] S. Mendach, R. Songmuang, S. Kiravittaya, A. Rastelli, M. Benyoucef, and O. G. Schmidt, Appl. Phys. Lett. **88**, 111120 (2006).
[8] S. Mendach, O. Schumacher, H. Welsch, Ch. Heyn, W. Hansen, and M. Holz, Appl. Phys. Lett. **88**, 212113 (2006).
[9] N. Shaji, H. Qin, R. H. Blick, L. J. Klein, Ch. Deneke, and O. G. Schmidt, Appl. Phys. Lett. **90**, 042101 (2007).
[10] S. Mendach, S. Kiravittaya, A. Rastelli, M. Benyoucef, R. Songmuang, and O. G. Schmidt, Phys. Rev. B **78**, 035317 (2008).
[11] T. Kipp, H. Welsch, Ch. Strelow, Ch. Heyn, and D. Heitmann, Phys. Rev. Lett. **96**, 077403 (2006).
[12] R. Songmuang, A. Rastelli, S. Mendach, and O. G. Schmidt, Appl. Phys. Lett. **90**, 091905 (2007).
[13] A. Bernardi, S. Kiravittaya, A. Rastelli, R. Songmuang, D. J. Thurmer, M. Benyoucef, and O. G. Schmidt, Appl. Phys. Lett. **93**, 094106 (2008).
[14] Ch. Deneke and O. G. Schmidt, Appl. Phys. Lett. **85**, 2914 (2004).
[15] D. J. Thurmer and Ch. Deneke, Yongfeng Mei, O. G. Schmidt, Appl. Phys. Lett. **89**, 223507 (2006).
[16] D. Grutzmacher, L. Zhang, L. Dong, D. Bell, B. Nelson, A. Prinz, and E. Ruh, Microelectron. J. **39**, 478 (2008).
[17] L. Zhang, L. Dong, and B. J. Nelson, Appl. Phys. Lett. **92**, 243102 (2008).
[18] R. Songmuang, Ch. Deneke, and O. G. Schmidt, Appl. Phys. Lett. **89**, 223109 (2006).
[19] Ch. Deneke, U. Zschieschang, H. Klauk, and O. G. Schmidt, Appl. Phys. Lett. **89**, 263110 (2006).
[20] Ch. Deneke, W. Sigle, U. Eigenthaler, P. A. van Aken, G. Schütz, and O. G. Schmidt, Appl. Phys. Lett. **90**, 263107 (2007).
[21] F. Cavallo, W. Sigle, and O. G. Schmidt, J. Appl. Phys. **103**, 116103 (2008).
[22] A. Bernardi, A. R. Goñi, M. I. Alonso, F. Alsina, H. Scheel, P. O. Vaccaro, and N. Saito, J. Appl. Phys. **99**, 063512 (2006).
[23] R. Songmuang, N. Y. Jin-Phillipp, S. Mendach, and O. G. Schmidt, Appl. Phys. Lett. **88**, 021913 (2006).
[24] F. Cavallo, R. Songmuang, C. Ulrich, and O. G. Schmidt, Appl. Phys. Lett. **90**, 193120 (2007).
[25] B. Krause, C. Mocuta, T. H. Metzger, Ch. Deneke, and O. G. Schmidt, Phys. Rev. Lett. **96**, 165502 (2006).
[26] Ch. Deneke, C. Muller, N. Y. Jin-Phillipp, and O. G. Schmidt, Semicond. Sci. Technol. **17**, 1278 (2002).
[27] G. P. Nikishkov, J. Appl. Phys. **94**, 5333 (2003).
[28] Pei Chi Chou and Nicholas J. Pagano, *Elasticity: Tensor, Dyadic, and Engineering Approaches* (Dover, New York, 1992).
[29] M. Grundmann, Appl. Phys. Lett. **83**, 2444 (2003).
[30] H. Morkoç, B. Sverdlov, and Guang-b Gao, Proc. IEEE **81**, 493 (1993).
[31] L. G. Parratt, Phys. Rev. **95**, 359 (1954). Here we have used PARRATT32 software to fit the experimental reflectivity datasets.
[32] A. Rastelli, A. Ulhaq, Ch. Deneke, L. Wang, M. Benyoucef, E. Coric, W. Winter, S. Mendach, F. Horton, F. Cavallo, T. Merdzhanova, S. Kiravittaya, and O. G. Schmidt, Phys. Status Solidi C **3**, 3641 (2006).
[33] Y. Mei, D. J. Thurmer, F. Cavallo, S. Kiravittaya, and O. G. Schmidt, Adv. Mater. (Weinheim, Ger.) **19**, 2124 (2007).
[34] C. Mocuta, J. Stangl, K. Mondboth, T. H. Metzger, G. Bauer, I. A. Vartanyants, M. Schmidbauer, and T. Boeck, Phys. Rev. B **77**, 245425 (2008).
[35] In order to precisely determine the out-of-plane lattice parameter and composition of the flat pseudomorphically strained $In_xAl_yGa_{1-x-y}As$ films from x-ray radial scans, a fit using dynamical diffraction theory would be needed. In this work the small deviation from the lattice parameter extracted from the diffraction peak position (smaller than 30 arc sec) to the actual $a_\perp$ value was included in the error bar, while the In content in the layers is assumed as nominal, within an error bar of 0.5%.
[36] G. Renaud, A. Barbier, and O. Robach, Phys. Rev. B **60**, 5872 (1999).
[37] B. E. Warren, *X-ray diffraction* (Dover, New York, 1969).
[38] Ch. Deneke, N.-Y. Jin-Phillipp, I. Loa, and O. G. Schmidt, Appl. Phys. Lett. **84**, 4475 (2004).
[39] Ch. Deneke, Ph. D. Thesis, University of Stuttgart, 2005.
[40] F. Cavallo, R. Songmuang, C. Ulrich, and O. G. Schmidt, Appl. Phys. Lett. **90**, 193120 (2007).
[41] L. Lazzarini, L. Nasi, C. E. Norman, and G. Salviati, J. Cryst. Growth **126**, 133 (1993).